Experimental Investigation of Axial Pull-out Behavior of Glued-in Threaded Rods in Cross-Laminated Timber

Zhibin Ling,[a,b,*] Zheng Li,[a,c] Zhoujun Li,[d] Chao Yang,[e] Wei Zheng,[f] and Lingfeng Zhang [g]

Cross-laminated timber (CLT), known for its high performance, prefabrication, low carbon emission, and eco-friendliness, has gained widespread adoption in the construction industry. Glued-in rod (GiR) connections, which offer a concealed appearance, high strength, withdrawal stiffness, ease of construction, and fire resistance, have become a promising solution for CLT structures. This study experimentally investigated the axial pull-out behavior of GiR connections in CLT. Forty-five CLT specimens with single GiR were designed and tested under pull-out conditions. The experimental variables included embedment length, threaded rod diameter, and rod-to-grain angle (parallel and perpendicular). The results revealed that CLT connections with GiR parallel to the grain exhibited an ascending load-slip response until peak load, followed by a sudden failure, while those with GiR perpendicular to the grain showed a linear increase to peak load with a subsequent gradual load reduction. Increasing the embedment length from 5 *d* to 15 *d* enhanced the pull-out load but decreased the average bond stress. Additionally, larger rod diameters led to higher pull-out loads and withdrawal stiffness within a certain range but reduced the average bond stress. The study also evaluated the effectiveness of existing bond stress-slip models and pull-out load prediction models for GiR connections in CLT, providing a foundation for future standardization efforts.

DOI: 10.15376/biores.20.3.5407-5428

Keywords: Cross-laminated timber; Glued-in rod; Bond behavior; Pull-out load; Withdrawal stiffness; Bond-slip behavior

Contact information: a: School of Civil Engineering, Suzhou University of Science and Technology, Suzhou 215011, P. R. China; b: Key Laboratory of Building Structural Retrofitting & Underground Space Engineering (Shandong Jianzhu University), Ministry of Education, Jinan250101, P. R. China; c: College of Material Science and Engineering, Northeast Forestry University, Harbin 150040, China; d: Shanghai Jianke Technical Assessment of Construction Co., Ltd, Shanghai 201108, P. R. China; e: College of Mechanical and Electrical Engineering, Northeast Forestry University, Harbin 150040, China; f: College of Materials and Science Engineering, Nanjing Forestry University, Nanjing 210037, P. R. China; g: College of Civil Science and Engineering, Yangzhou University, Yangzhou 225127, P. R. China;
** Corresponding author: zbling@mail.usts.edu.cn*

INTRODUCTION

Cross-laminated timber (CLT) was initially introduced in Europe and has since been adopted globally as a high-performance, prefabricated, low-carbon-emission, and eco-friendly construction material with outstanding dimensional stability. Beyond its common use in walls and floors, CLT has become a critical material in contemporary construction, often combined with other materials to create extended spans and taller structures (Sofi *et al*. 2021). In these applications, the CLT structures demand connections

with significantly higher load-carrying capacity and stiffness than conventional timber joints, especially in tall buildings and large-span scenarios.

In recent years, glued-in rod (GiR) timber connections have gained significant attention on account of their concealed appearance, high strength, withdrawal stiffness, ease of construction, and fire-resistant properties (Zhang *et al*. 2023). Although GiR connections have been successfully implemented in glued laminated timber (glulam) and laminated veneer lumber (LVL) structures, no unified design provision exists worldwide. Given the proven effectiveness of GiR techniques in glulam and LVL, they are considered a promising connector solution for CLT structures. Potential applications include wall-to-foundation connections, spliced wall-wall joints, and beam-to-wall linkages. To standardize GiR design, initiatives such as the GIROD project (Gustafsson and Serrano 2002) and German DIN 1052:2004-08 (2008) and New Zealand codes (Buchanan 2007) have been conducted consequently (Tlustochowicz *et al*. 2010).

The axial pull-out behavior of GiR connections is critical for ensuring the structural integrity and reliability of structures, as it directly affects the load-carrying capacity and failure modes of the connections. Previous studies on GiR connections in various timber products have been conducted over the past three decades. These studies have employed theoretical derivations (Gardelle and Morlier 2006; Hassanieh *et al*. 2018), numerical simulations (Lartigau *et al*. 2014; Coureau *et al*. 2016; Madhoushi and Ansell 2017; Grunwald *et al*. 2019), and experimental investigations (Tannert *et al*. 2016; Myslicki *et al*. 2019)). For solid timber, Otero Chans *et al.* (2009, 2011, 2013) conducted extensive research on the strength and behavior of GiR connections. In glulam, Rossignon and Espion (2008) and Ling *et al.* (2014, 2019) focused on the pull-out strength and bond behavior of GiR connections. Stepinac *et al.* (2016) and Myslicki *et al.* (2018) investigated GiR connections in laminated veneer lumber (LVL).

Research on GiR connections in CLT remains relatively limited, both in terms the of scope of conclusions and the volume of studies conducted. Rajčić *et al*. (2006) demonstrated that GiR connections in CLT exhibit significantly lower pull-out strength and distinct failure modes compared to glulam counterparts. Koets (2012) conducted pull-out tests to analyze adhesive types and rod-grain angles, proposing empirical formulae that require further validation. Azinovic *et al*. (2018, 2019) identified failure mode dependencies and load-capacity relationships with embedment length and rod diameter through 60 pull-pull tests and numerical simulations, noting stress distribution similarities to glulam connections. Sofi *et al*. (2021) further validated these findings through 30 pull-pull tests, highlighting discrepancies between experimental results and existing design equations. However, research on GiR connections in CLT remains limited, with insufficient data and unresolved failure mechanisms, thus hindering broader application. To address these gaps, this study investigates the influence of CLT cross-layers on the pull-out behavior of GiR connections.

To investigate the influence of CLT cross-layers on GiR pull-out behavior, forty-five CLT specimens with rods embedded parallel and perpendicular to the grain were designed. The pull-out configuration (Muciaccia 2017) was adopted to analyze bond-slip relationships and mechanical performance. Experimental results were compared with existing prediction models to assess their validity, providing a foundation for future standardization efforts.

EXPERIMENTAL

Material Properties

Timber

For this study, Spruce-pine-fir CLT panels, which consist of three layers of laminates and are classified as C24 (Borgström and Fröbel 2019), were utilized. These panels were produced by Ningbo Sino-Canada Low-Carbon New Technology Research Institute Ltd. The total thickness of CLT panels is 105 mm, allocating 35 mm to each layer. The mechanical properties of lamellae of CLT are presented in Table 1. The strength classes are as defined by Gagnon and Pîrvu (2011). The mean density of CLT was measured as 410.5 kg/m^3. The moisture content of CLT was obtained as 12% according to GB/T 1927.4-2021 (2021). Test diagram of CLT specimen is presented in Fig. 1.

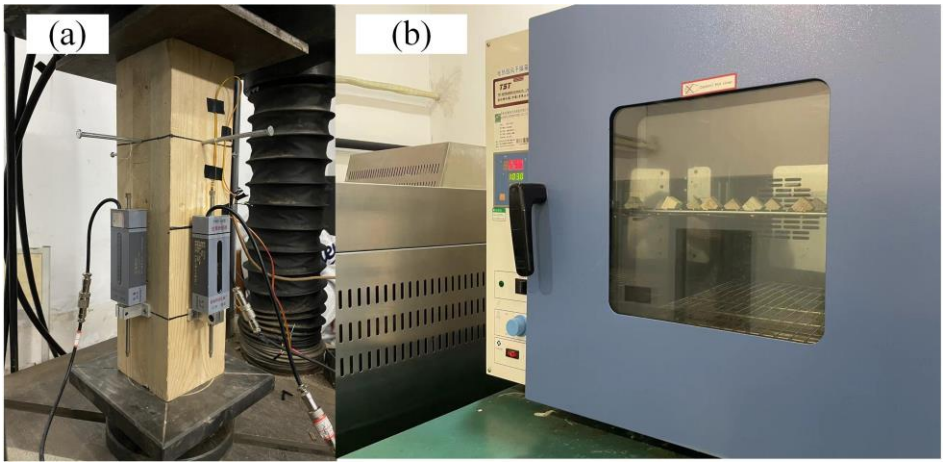

Fig. 1. Test diagram of CLT specimen: (a) compression test; and (b) Moisture content test

Table 1. Mechanical Properties of Lamellae of CLT

Strength Class	Bending Strength $f_{m,k}$ (MPa)	Tensile Strength Parallel to the Grain $f_{t,0,k}$ (MPa)	Tensile Strength Perpendicular to the Grain $f_{t,90,k}$ (MPa)	Shear Strength $f_{v,k}$ (MPa)	Rolling Shear Strength $f_{v,RS}$ (MPa)	Modulus of Elasticity Parallel to the Grain $E_{m,0,mean}$ (MPa)	Modulus of Elasticity Perpendicular to the Grain $E_{m,90,mean}$ (MPa)
C24	24	14.5	0.4	4.0	1.1	11000	370

Threaded rods

Grade 8.8 threaded rods were chosen as the GiR in this study. The mechanical properties of GiR reported in Table 2 were obtained by the manufacturer in accordance with the Chinese standard GB/T 3098.1-2010 (2010) for tensile testing of metal materials.

Table 2. Mechanical Properties of Threaded Rods

Properties	Value (MPa)
Modulus of Elasticity	211200
Yield Strength	662
Tensile Strength	834

Adhesive

Two-component epoxy resin was selected as the adhesive herein due to its good environmental adaptability and stable bonding performance. The mechanical properties of the adhesive were provided by the manufacturer and were determined according to (GB/T 7124-2008), as shown in Table 3.

Table 3. Mechanical Properties of Adhesive

Properties	Value (MPa)
Splitting Strength	19.57
Compressive Strength	107.6
Bond Strength	19.2

Specimens and Testing Procedure

Five replicates were prepared for each group of specimens considering the discreteness of test results. The specimens featured a cross-section size of 105 mm × 105 mm, a length of 400 mm, and an edge distance of 3.28*d*, meeting the minimum edge distance recommendation of 2.5 *d* found in the literature (Steiger *et al*. 2015), as shown in Fig. 2. The pre-drilled holes were cleaned with a brush in order to remove all debris and dust. The epoxy adhesive was then injected into the holes with two-thirds of the hole volume filled empirically. The rod was inserted into the partially epoxy-filled hole while twisting to remove any air bubbles so that the adhesive was evenly distributed along the length of hole. All the specimens were cured at a constant room temperature for one week before testing. The specimen group code was labelled as Specimen (S)-Nominal Diameter-Embedded Length-Parallel (P) or Perpendicular (PP) to the grain, as shown in Table 4.

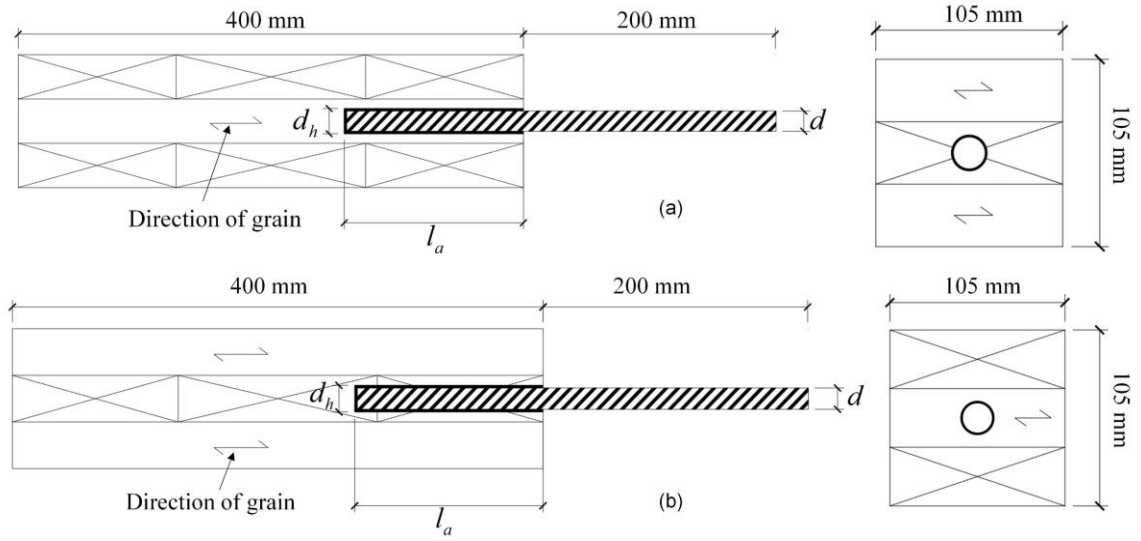

Fig. 2. Schematic diagram of specimen: (a) Parallel to the grain; and (b) perpendicular to the grain.

Figure 3 illustrates the set-up of pull-out tests. A steel frame consisting of two thick steel plates connected by four steel rods was designed to transfer the load from the jaws of the machine to the specimen, with a hinge joint on the top of the frame. It is worth mentioning that the pull-out test configuration might repress the pull-out failure of cross layer for the CLT specimens with GiR, which is a drawback of the test setup for the pull-

out tests of GiR in CLT. Although this configuration may affect the pull-out strength of the connections, the selection of the minimum edge distance avoids longitudinal splitting of timber and reduces the effect of compression on the pull-out strength to a certain extent (Shekarchi *et al*. 2019; Navaratnam *et al*. 2022).

Table 4. List of Specimens

Specimen Group Code	*d* (mm)	L_a (mm)	λ	*t* (mm)	Orientation	*L* (mm)	Number of Replicates
S12-60-P	12	60	5	2	P	400	5
S12-120-P	12	120	10	2	P	400	5
S12-180-P	12	180	15	2	P	400	5
S16-80-P	16	80	5	2	P	400	5
S16-160-P	16	160	10	2	P	400	5
S16-240-P	16	240	15	2	P	400	5
S16-80-PP	16	80	5	2	PP	400	5
S16-160-PP	16	160	10	2	PP	400	5
S16-240-PP	16	240	15	2	PP	400	5

Note: L = Total length of CLT block, d = Nominal diameter of threaded rod, L_a = Embedment length, $\lambda = L_a / d$, and t = Thickness of adhesive layer.

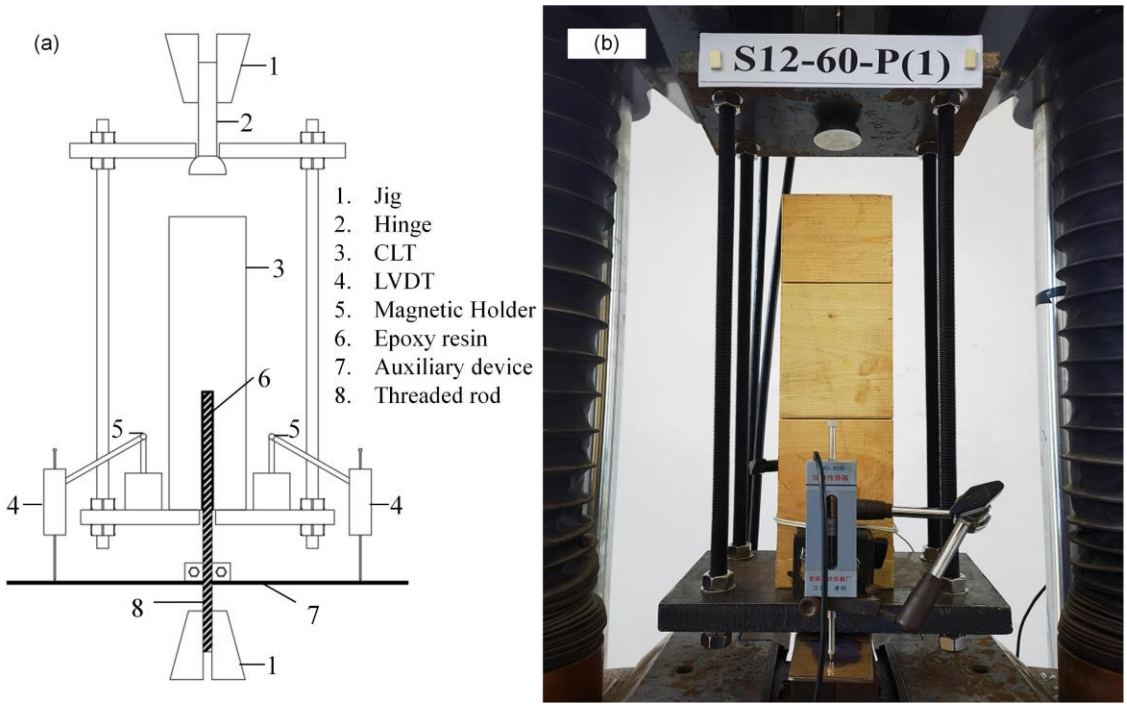

Fig. 3. Test set-up: (a) Schematic; and (b) photograph

All the tests were carried out on a hydraulic universal testing machine with a capacity of 1000 kN. The loading rate was set as a constant of 0.5 mm/min to failure of specimens with a reference of (ASTM D1761-20, 2006). Two linear voltage displacement transducers (LVDTs) were symmetrically arranged on both sides of the specimen to measure the relative slip between the CLT and the GiR, and the average value of the experimentally recorded displacements was taken as the slip value of the specimens.

RESULTS

Typical Failure Modes

Four failure modes were identified (Fig. 4): (a) Timber-adhesive interface shear failure (adhesive layer fracture or fiber extraction from the adhesive interface), (b) Plug pull-out failure (timber shear failure along the rod axis), (c) Mixed failure (combined adhesive shear and localized timber fiber fracture), and (d) Splitting failure (longitudinal timber cracking due to rolling shear in cross-layers). The timber-adhesive interface shear failure, as the predominant mode in the specimens with GiR parallel to the grain (P-specimens) with 5 *d* embedment length, indicated either the breakage of adhesive layer or the extraction of timber fiber attached at the adhesive layer as the rod was pulled out, as depicted in Fig. 4a which is consistent with the literature (Sofi *et al*. 2021).

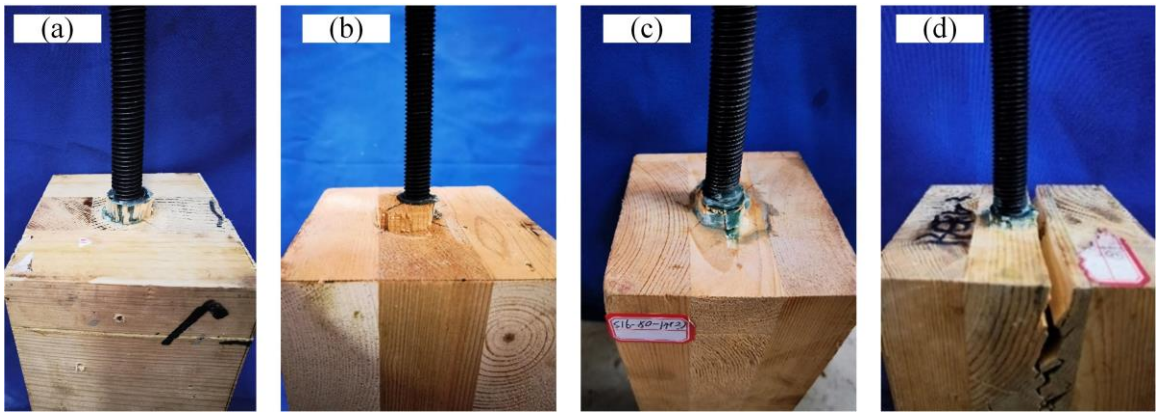

Fig. 4. Typical failure modes of specimens: (a) Timber-adhesive interface shear failure; (b) plug pull-out failure of timber; (c) mixed failure combining shear failure of adhesive layer and timber shear failure; and (d) splitting failure of the cross layer in CLT

Table 5 indicates that plug pull-out failure of timber indicating timber shear failure also occurred in the specimens with GiR parallel to the grain, as evidenced in Fig. 4b. Plug shear failure usually occurred in the timber connections with GiR parallel to the grain in previous studies (Azinović *et al*. 2018), and although the loading configuration used in this study prevents further expansion of this failure mode, the trend of the evolution of the failure mode as a whole can still be clearly seen. Overall, the concerning damage pattern of timber splitting was almost absent in the failure modes of P-specimens. In the case of the specimens with GiR perpendicular to the grain (PP-specimens), a mixed failure pattern typically appeared (Fig. 4c), with timber fibers fracturing around the holes (fiber breakage perpendicular to the grain) occurring irregularly. With the increase of embedment length, the failure mode of the specimen was more unstable, as evidenced by splitting of the timber along the bond-line direction (Fig. 4d). This highlighted a strong correlation between the

failure of PP-specimens and timber material properties, indicating the importance of rolling shear strength in the failure of specimens perpendicular to the grain (Hegeir and Stamatopoulos 2023).

Load-slip Behavior

Figure 5 shows the individual and average load-slip curves for each group of specimens. For the specimens with GiR parallel to the grain (Figs. 5a-5f), the curves exhibited a linear rise at the initial loading stage, followed by a nonlinear slip between the rod and CLT as the load increased to a sudden drop load, which indicated that brittle failure had occurred. Discreteness among the curves in Figs. 5a-5f was observed especially for the S12-180-P(4) and S16-80-P(4) specimens.

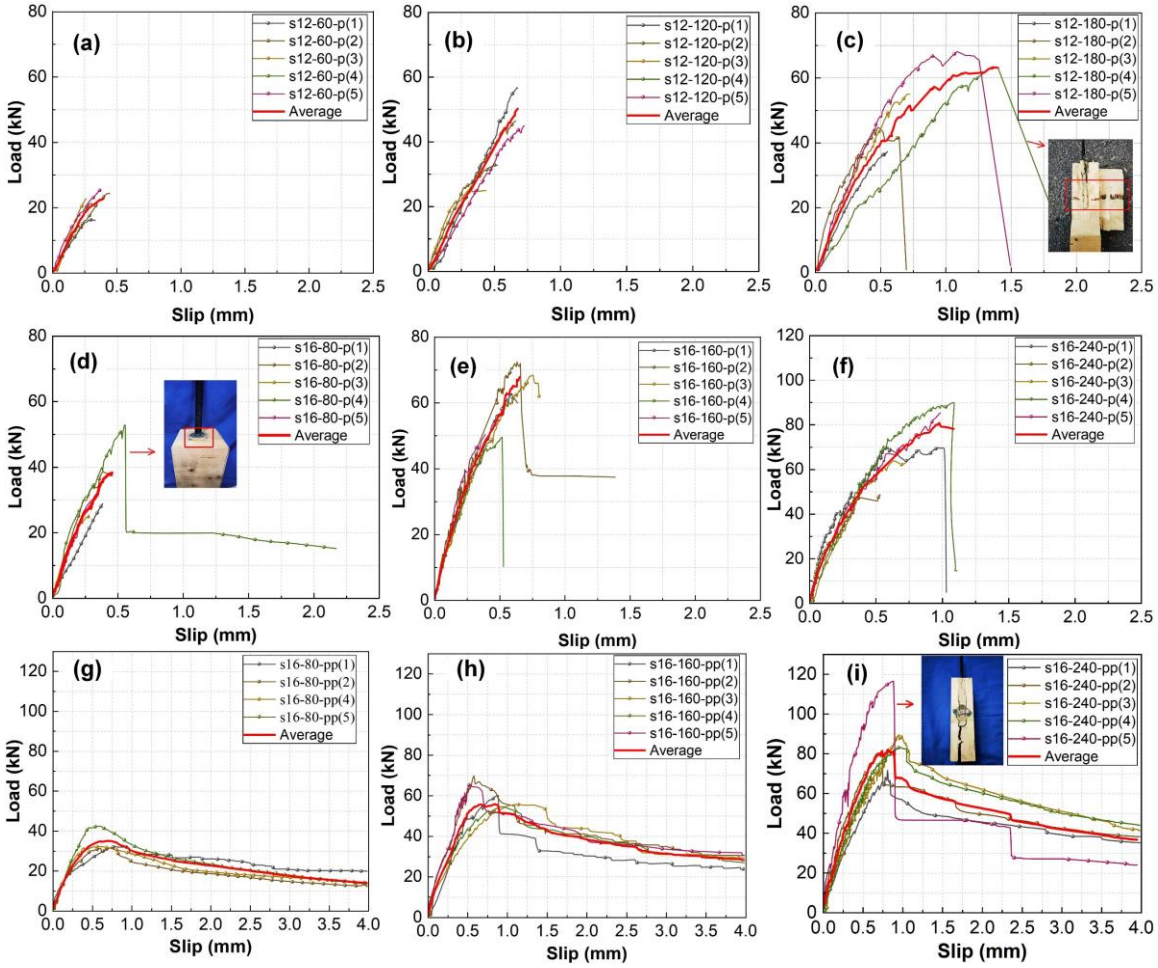

Fig. 5. Load-slip curves: (a) S12-60-P; (b) S12-120-P; (c) S12-180-P; (d) S16-80-P; (e) S16-160-P; (f) S16-240-P; (g) S16-80-PP; (h) S16-160-PP; and (i) S16-240-PP

Specimen S12-180-P (4) shows a relatively lower withdrawal capacity at the same slip level, which might be due to internal defects, as illustrated in Fig. 5c. The specimen S16-80-P (4) exhibited a circular shear failure interface, which was attributed to restraint from the loading configuration. Subsequent separation of the rod from the lumber was performed, and it was found that this specimen had a higher degree of adhesion than the rest of the specimens in the same group. In general, the load-slip curves of the specimens with GiR perpendicular to the grain (Figs. 5g-5i) generally show a linearly increasing

response to peak load followed by a post-peak gradual decrease. It is worth noting that the withdrawal capacity of S16-240-PP (5) was obviously higher than that of the other specimens in the same group, as shown in Fig 4i. The presence of insect-induced holes in timber can result in the formation of adhesive accumulation within the bottom cavities during the gluing process. This occurrence has the potential to influence the bond integrity of GiR, thereby necessitating careful consideration in the evaluation of structural performance and durability (Estévez Cimadevila *et al*. 2013).

Table 5. Summary of Experimental Values

Specimen Code	F_{ult} (kN)	s_m (mm)	K (kN/mm)	τ_a (MPa)	Failure Modes
S12-60-P	21.82 (16%)*	0.34 (21%)	91.08 (29%)	9.65 (16%)	4A+1B
S12-120-P	41.06 (30%)	0.58 (28%)	100.62 (20%)	9.08 (30%)	2A+3B
S12-180-P	52.74 (25%)	0.88 (40%)	106.37 (36%)	7.78 (25%)	1A+4B
S16-80-P	35.39 (31%)	0.39 (28%)	138.22 (42%)	8.81 (31%)	3A+2B
S16-160-P	60.64 (17%)	0.64 (34%)	145.44 (14%)	7.54 (17%)	2A+2B+1D
S16-240-P	71.59 (24%)	0.85 (29%)	186.33 (28%)	5.94 (24%)	1A+4B
S16-80-PP	34.23 (15%)	0.68 (15%)	105.06 (7%)	8.52 (15%)	4C
S16-160-PP	60.90 (11%)	0.81 (30%)	115.28 (26%)	7.58 (11%)	2C+3D
S16-240-PP	88.20 (19%)	0.87 (12%)	140.77 (23%)	7.32 (19%)	1C+4D

*The bracketed values are coefficient of variation (CoV). A= timber-adhesive interface shear failure; B= plug pull-out failure of timber; C= mixed failure combining shear failure of adhesive layer and timber shear failure; and D= splitting failure of cross layer in CLT.

The main test results are presented in Table 5. It should be noted that the group S16-80-PP in Table 5 only has four individual specimens, since the specimen S16-80-PP(3) failed prematurely. F_{ult} indicates the pull-out load (kN) of specimens. s_m means the slip at the loaded end (mm) corresponding to F_{ult}, and K is the initial stiffness (kN/mm) calculated according to Eq. 1. In addition, the average bond stress τ_a (MPa)at timber/adhesive is determined based on Eq. 2.

$$K = \frac{0.4F_{ult} - 0.1F_{ult}}{s_{0.4} - s_{0.1}} \quad (1)$$

$$\tau_a = F_{ult} / \left(\pi \cdot d_h \cdot l_a\right) \quad (2)$$

In Eq. 2, d_h is the diameter (mm) of the hole, as shown in Fig. 2.

It is apparent that there were discrete characteristics of the same series of specimens, which further illustrates the necessity of investigating the pull-out behavior of GiR connection in CLT. In summary, the pull-out load, the slip corresponding to the pull-out load, and the withdrawal stiffness increased with the embedment length increasing, while the bond stress decreased. The coefficient of variation for pull-out load ranged from

11% to 30%, showing moderate variability in load-bearing capacity within each group. The withdrawal stiffness exhibited relatively higher variation compared to pull-out load, especially in the S16-80-P group (42%) and the S12-120-P group (36%), indicating that the properties of CLT greatly affected the withdrawal stiffness of the GiR in the CLT.

DISCUSSION

Effect of Embedment Length

The embedment length was confirmed as a critical factor influencing the pull-out behavior of GiR connections. To facilitate comparison, the embedment length-to-diameter ratio ($\lambda = l_a / d$) was adopted to assess its impact on the mechanical behavior of the connections, in line with previous literature (Steiger *et al*. 2006; Zhu *et al*. 2017). Figure 6 illustrates the connection behavior at varying ratio of embedment length to diameter. For both the S12 and S16 specimen series, the results indicate that within a specific range, increased embedment length corresponded to higher pull-out load. The increase in pull-out load was more pronounced when the embedment length was extended from 5 *d* to 10 *d* compared to the increment from 10 *d* to 15 *d*, a finding consistent with prior studies (Ayansola *et al*. 2022; Vallée *et al*. 2022). As the embedment length increased, the failure mode evolved from wood fiber shear failure at the bond line to timber block shear failure, an undesirable mode that may compromise connection reliability. No rod yielding was observed in this study, as high-strength steel rods were used to prevent ductile failure modes. Consequently, low-yield-point steel rods are recommended for timber connections to enhance ductility.

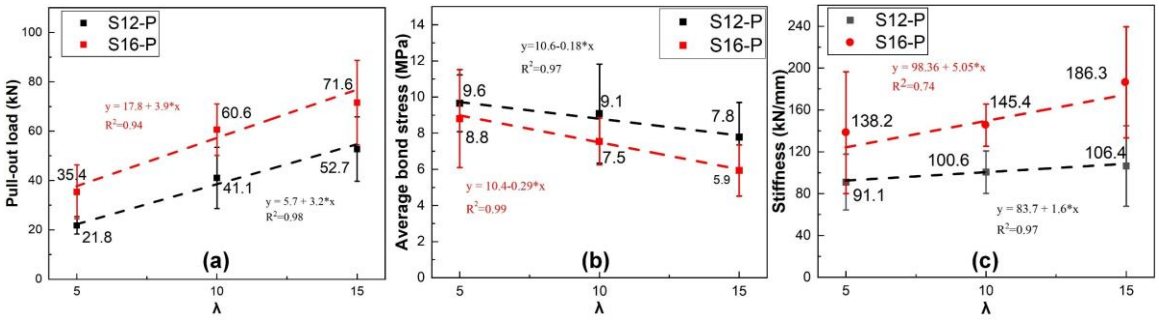

Fig. 6. Connection behavior at different embedment length: (a) Pull-out load; (b) Average bond stress; and (c) Stiffness

Figure 6b shows that the average bond stress decreases approximately linearly as the embedment length increased, and the dotted line in the figure indicates the linearly fitted decreasing equation and provides the corresponding R^2 value. This phenomenon was also observed in previous studies regarding the conventional GiR connections in other kinds of timber products (Siha and Zhou 2021). It can be observed from Table 5 that the degree of dispersion was affected by the failure mode, and the failure of timber results in a deviation of pull-out load from the global tendency. The specimens with an embedment length of 10 *d* showed a minimum deviation of withdrawal stiffness, as shown in Fig. 6c. It can be preliminarily inferred from 10 *d* is supposed to the threshold value of embedment length from the failure of P-specimens changed from adhesive layer fracture to timber failure.

The embedment length was confirmed as a critical factor influencing the withdrawal stiffness of GiR connections. While previous studies on GiR in glulam (Steiger *et al.* 2006) and LVL (Stepinac *et al.* 2016) have reported similar trends for embedment length effects, the CLT cross-layers introduce distinct failure mechanisms. For instance, Azinović *et al.* (2018) observed that withdrawal stiffness in glulam remains stable with increased embedment length, whereas the S16-P group in CLT exhibited significant stiffness variations (Fig. 6c). This discrepancy highlights the unique influence of orthotropic structure on bond stress distribution of CLT, a phenomenon not extensively addressed in prior literature. Additionally, the transition from adhesive failure to timber shear failure at 10 *d* embedment length (Fig. 6b) contrasts with the findings of Sofi *et al.* (2021), who reported adhesive-dominated failures in CLT even at longer embedment lengths, underscoring the need for CLT-specific design guidelines.

Effect of Rod-to-Grain Angle

The effect of the rod-to-grain angle on the connection behavior is presented in Fig 7. The pull-out load was generally in a linear proportion to embedment length for both the P- and PP- series of specimens, as shown in Fig. 7a. At shorter embedment lengths (5 *d*), the pull-out load of P-specimens exceeded that of PP-specimens. However, as the embedment length increased to 10 *d* and further to 15 *d*, the bearing capacity of PP-specimens surpassed that of P-specimens, a trend consistent with prior literature (Azinović *et al*. 2018).

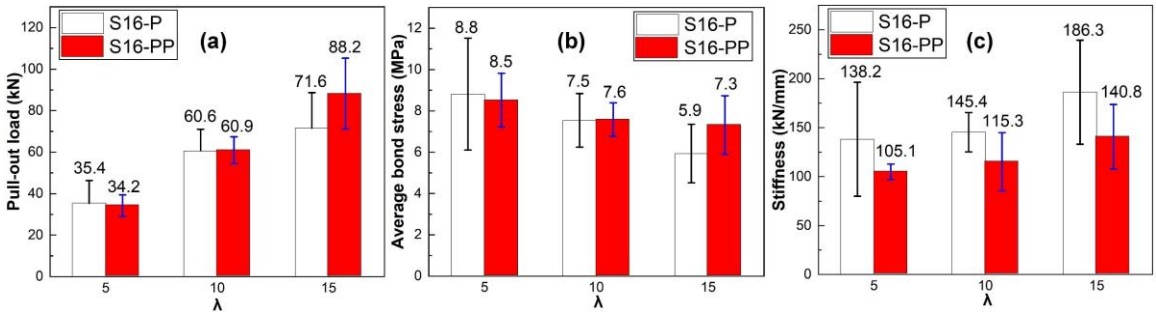

Fig. 7. Connection behavior of specimens with different rod-to-grain angle: (a) pull-out load; (b) average bond stress; and (c) stiffness.

Figure 7b illustrates that the average bond stress for both P and PP specimens decreased gradually as the embedment length increased from 5 *d* to 15 *d*. Specifically, for P specimens, the average bond stress decreased by 15% when the embedment length increased from 5 *d* to 10 *d*, and by an additional 25% when extended to 15 *d*. In contrast, for PP specimens, the average bond stress decreased by 10% from 5 *d* to 10 *d*, and only by 3% from 10 *d* to 15 *d*. This indicates that increasing the embedment length was more effective in reducing average bond stress and promoting ductile failure in P specimens compared to PP specimens. For PP specimens, the increase in embedment length did not significantly affect the average bond stress and led to more pronounced rolling shear failure of the wood, as detailed in Table 5. Moreover, the increase in embedment length had a minimal effect on improving the withdrawal stiffness of PP specimens, as shown in Fig. 7. The failure modes for PP specimens at medium and long embedment lengths (10 *d* and 15 *d*) were less desirable. Based on these findings, it is recommended to glue rods in parallel

lamellas in CLT structures to ensure reliable load capacity and relatively high withdrawal stiffness in practical applications.

Effect of Rod Diameter

Figure 8 shows the effect of rod diameter on the behavior of the GiR connections in CLT including pull-out load, average bond stresses, and withdrawal stiffness. The pull-out load of the S16-P specimen group was 62%, 47%, and 35% higher than that of the S12-P specimen group at the embedment length of 5 *d*, 10 *d*, and 15 *d*, respectively. Meanwhile, the average bond stress of the specimen group S16-P decreased by 8%, 17%, and 23% at the embedment length of 5 *d*, 10 *d*, and 15 *d*, respectively compared to the specimen group S12-P indicating the larger rod diameter, the relatively lower bond stress level in a certain range. Also, increasing the rod diameter improves the withdrawal stiffness of the connection moderately, with a corresponding increase in result deviation, as shown Fig. 8c.

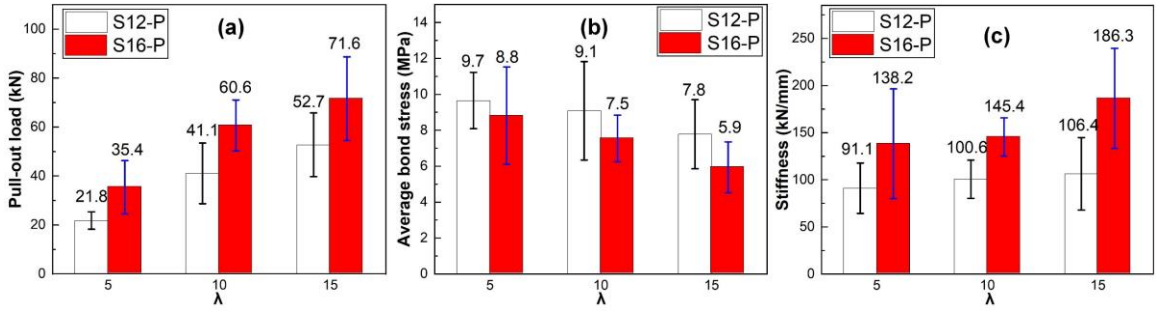

Fig. 8. Connection behavior of specimens with different rod diameter: (a) Pull-out load; (b) Average bond stress; and (c) Stiffness.

Analytical Bond Stress–Slip Relationship

Over the past few decades, several bond-slip models have been proposed to elaborate the interfacial bond-slip behavior between steel or fiber-reinforced polymer (FRP) and concrete. These models can provide guidance for predicting the bond-slip relationship of the GiR connections in CLT.

Cosenza *et al*. (1997) proposed the Cosenza-Manfredi-Realfonzo (CMR) model expressed as Eq. 3 to predict the bond stress-slip relationship between concrete and FRP bar. It should be noted that the CMR model only has an ascending branch, indicating that the CMR model is suitable for the case of brittle bond failure. The literature (Siha and Zhou 2021) indicates the CMR model can be used to predict the bond stress-slip relationship of the GiR timber connections effectively. Due to the GiR connections in CLT parallel to the grain mainly failed by brittle failure, the CMR model was used to predict the bond-slip relationship of the GiR connections in CLT parallel to the grain herein, as shown in Eq. 3,

$$\frac{\tau}{\tau_m} = (1 - \exp(-\frac{s}{s_r}))^{\beta} \quad 0 \le s \le s_m \tag{3}$$

where s_r and β are the parameters obtained from curve fitting of experimental results. For $L_a \le 10d$, $s_r = 0.2$ and $\beta = 1.4$, while for $L_a > 10d$, $s_r = 0.3$ and $\beta = 1.3$ in this study.

Table 6. Parameters of the Bond Stress-Slip Relationship

Specimen Group Code	α	β
S16-80-PP	0.64	0.32
S16-160-PP	0.66	0.42
S16-240-PP	0.72	0.56

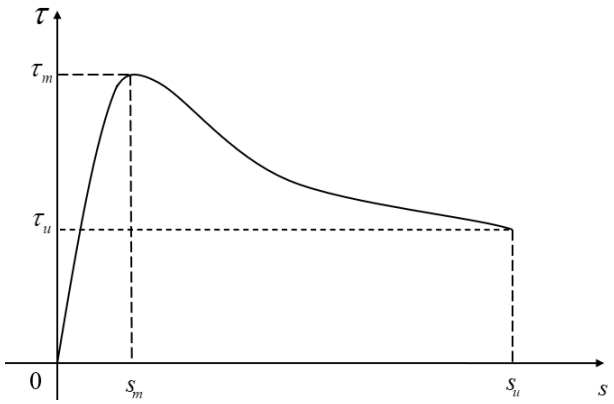

Fig. 9. Partially modified BPE model by Ling *et al* (2014)

Given the significance of predicting the pseudo-ductility of GiR connections in timber, and recognizing that the CMR model only predicts the ascending branch, Ling *et al*. (2014, 2018) partially modified the BPE model (Eligehausen *et al*. 1983) to predict the bond-slip response of the GiR connections in glued laminated timber, as depicted in Fig. 9. This modified model by Ling *et al*. (2014) was selected to predict the bond stress-slip curve of the GiR connections in CLT perpendicular to the grain in this section, as expressed in Eq. 4,

$$\frac{\tau}{\tau_{\mathrm{m}}}=\begin{cases}\frac{1}{\alpha}\cdot(\frac{s}{s_{\mathrm{m}}})^{\alpha}-(\frac{1}{\alpha}-1)\cdot\frac{s}{s_{\mathrm{m}}} & 0\le s\le s_{\mathrm{m}}\\ \frac{s}{s_{\mathrm{m}}}\cdot\frac{1}{\frac{s}{s_{\mathrm{m}}}+\beta(\frac{s}{s_{\mathrm{m}}}-1)^{2}} & s>s_{\mathrm{m}}\end{cases} \quad (4)$$

where τ_{a} and s_{m} are the maximum bond stress and its corresponding slip. α and β are the parameters obtained from curve fitting of experimental results, listed in Table 6.

Figure 10 depicts the comparison between the theoretical bond stress-slip models and average experimental curves. It can be seen from Fig. 10a-10f that for the specimens with parallel-to-grain GiR connections in CLT, the predicted bond-slip curves showed good agreement with the experimental curves in the ascending branch indicating the CMR model can predict the ascending branch of GiR connections in CLT parallel to the grain effectively. Figure 10g-10i clearly shows that for the connection specimens with GiR perpendicular to the grain in CLT, the proposed bond-slip model proposed by Ling *et al*. (2014) generally fit the experimental curves well in both the ascending and the descending branches.

Predictions of Pull-out Load

This section aims to evaluate the feasibility of using existing theoretical models for predicting the pull-out strength of the GiR connection in CLT. The following prediction

models were chosen for comparisons, since most of the GiR connection specimens failed by bond failure or timber shear failure.

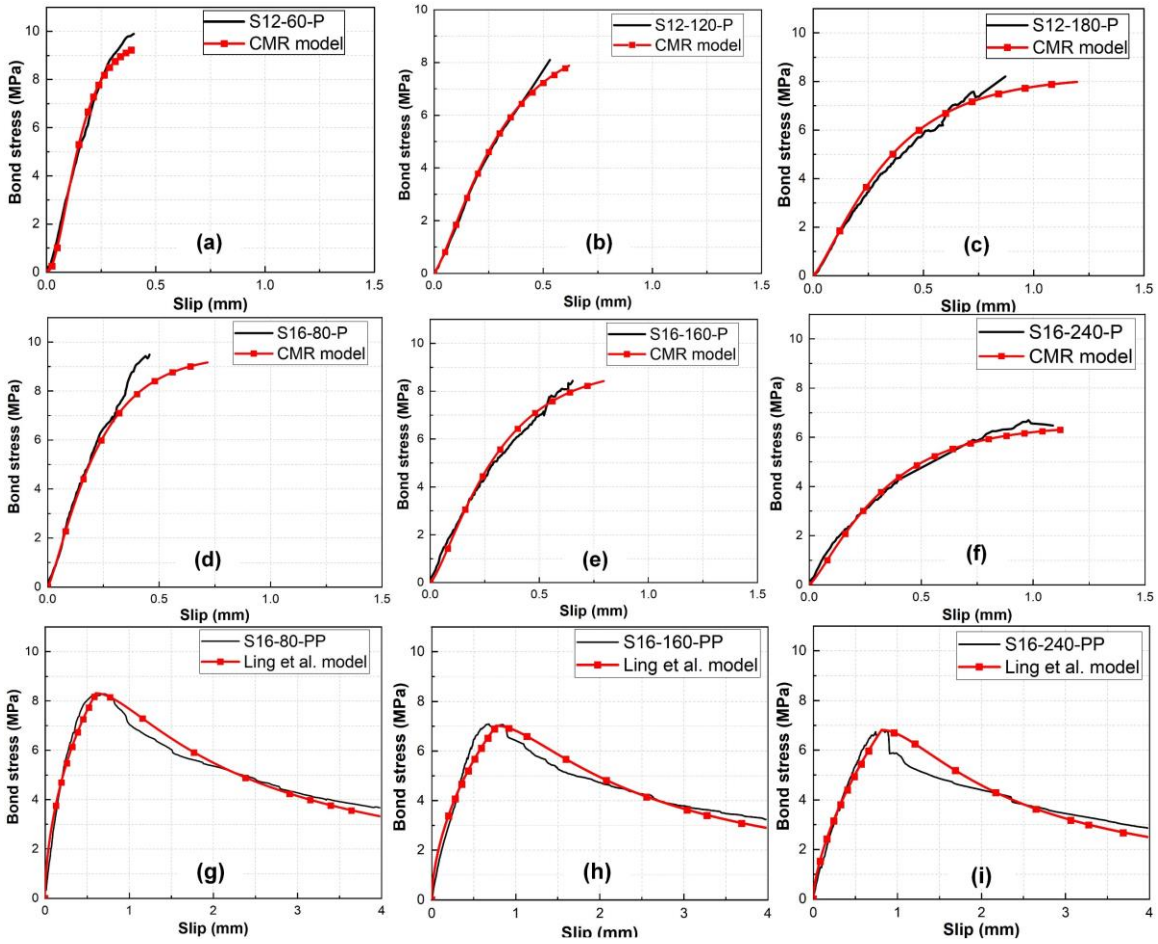

Fig. 10. Comparisons of analytical model with the average test curves

The GIROD Project Proposal

Bengtsson (2002) provided the design equations for the GIROD project. The theoretical equations are based on the GiR connections in glulam, where the thickness of the adhesive layer in the GiR specimens was 0.5 mm or less. The model was obtained based on a simplification of the pull-compressive loading configuration, as presented in Eq. 5:

$$F_G = \tau_f \cdot \pi \cdot d \cdot l \cdot (\tanh \omega) / \omega \tag{5}$$

where τ_f means the shear strength (MPa) of the adhesive,

$$\tau_f = \left[8129 \cdot d_h \cdot \lambda^{-0.62} \cdot (\rho / 480)^{0.5} \right] \tag{5a}$$

where ω indicates the stiffness ratio of the joint, and F_G represents mean axial capacity (N) of GiR connection. The relevant parameters are shown in Eq. 6,

$$\begin{aligned} \omega &= \sqrt{l_{geo} / l_m} \\ l_{geo} &= 1/2\pi dl^2 \cdot (1/A_r + (E_r / E_w)/A_w) \\ l_m &= E_r \cdot (G_f / \tau_f^2) \end{aligned} \tag{6}$$

where d =nominal diameter of rod (mm), l =embedment length (mm), A_r = the area of the rod (mm^2), A_w = the area of the wood (mm^2), E_r and E_w = the modulus of elasticity of the rod and wood (MPa), and G_r = fracture energy (J/m^2). The following values of parameters were assumed in this paper: $A_w = 110.25$ cm^2, E_w =10010 MPa, E_r =210000 MPa and G_f = 1750 J/m^2.

German Design Code DIN 1052: 2004-08

The design values for the load carrying capacity of GiR connections parallel and perpendicular to the grain are provided in the German design code for timber structures (DIN 1052:2004-08, 2008), as shown in Eq. 7:

$$R_{ax} = \pi d l_a f_{k1} \tag{7}$$

where l_a = embedment length (mm), and d = diameter of the rod (mm). The parameter R_{ax} represents characteristic axial capacity (N) of GiR connection. The value of f_{k1} is obtained from Eq. 8:

$$\begin{cases} f_{k1} = 4.0 & l_a \le 250mm \\ f_{k1} = 5.25 - 0.005 l_a & 250mm < l_a < 500mm \\ f_{k1} = 3.5 - 0.0015 l_a & 500mm < l_a \le 1000mm \end{cases} \tag{8}$$

Steiger, Widmann, and Gehri Proposal

Steiger *et al*. (2006) conducted a total of 48 pull-out tests of epoxy-based adhesives bonded GiR parallel to the grain in glulam. Then, the theoretical prediction model of the pull-out load was proposed accordingly based on the test results, as shown in Eq. 9:

$$\begin{aligned} F_S &= f_{v0,mean} \cdot \pi \cdot d_h \cdot l_a \\ f_{v0,mean} &= 7.8 \cdot (\lambda_h / 10)^{-1/3} \cdot (\rho / 480)^{0.6} \end{aligned} \tag{9}$$

In Eq. 9, $\lambda_h = l_a / d_h$, l_a means embedment length (mm), and d_h represents the diameter of the hole (mm). F_s represents characteristic axial capacity of GiR connection (N).

Widmann *et al*. (2007) investigated the pull-out properties of GiR connections perpendicular to the grain in glulam according to a similar experimental protocol and proposed a formula for calculating the pull-out load accordingly, as given in Eq. 10,

$$F_W = 0.045 \cdot \left(\pi \cdot d_h \cdot l_a\right)^{0.8} \tag{10}$$

where l_a means embedment length (mm), and d_h represents the diameter (mm) of the hole. The parameter F_w represents characteristic axial capacity (kN) of GiR connection.

New Zealand Design Guide

An equation to predict the pull-out load capacity of GiR connections parallel to the grain in glulam is provided in the New Zealand Design Guide (Buchanan 2007), as shown in Eq. 11:

$$F_{\mathrm{N}} = 6.73 \cdot k_{\mathrm{b}} \cdot k_{\mathrm{e}} \cdot k_{\mathrm{m}} \cdot (l_{\mathrm{a}} / d)^{0.86} \cdot (d / 20)^{1.62} \cdot (d_{\mathrm{h}} / d)^{0.5} \cdot (e' / d)^{0.5} \quad (11)$$

Here, the values of k_{b}, k_{e}, and k_{m} were calculated by the moisture content, type of rod, and adhesive, e' = edge distance (mm). The following values of parameters were assumed in this paper: $k_b = k_e = k_m = 1.0$. F_{N} represents characteristic axial capacity of GiR connection.

New Zealand Design Guide

Rossignol and Espion (2008) investigated the pull-out behavior of GiR connections in glulam with thicker adhesive layers. It was found that the failure mode was mainly timber splitting failure along the embedment length, and a semi-empirical formula was proposed to predict the pull-out load capacity of GiR connections parallel to the grain in timber, as depicted in Eq. 12,

$$\begin{aligned} F_{\mathrm{R0}} &= f_{\mathrm{ax,0,mean}} \cdot \pi \cdot d_{\mathrm{h}} \cdot l_{\mathrm{a}} \\ f_{\mathrm{ax,0,mean}} &= 5.8 \cdot (\lambda_{\mathrm{h}} / 10)^{-0.44} \end{aligned} \quad (12)$$

where $\lambda_{\mathrm{a}} = l_{\mathrm{a}} / d_h$, l_{a} represents the embedment length (mm).

Eurocode EN 17334-2021

Standard EN 17334 (2021) has been amended in accordance with Eurocode 5 Appendix (EN 1995-1-1, 2004) on glued rod connections to give the following prediction formulae, as shown in Eqs. 13 and 14:

$$F_{\mathrm{ax,Rd}} = \min \begin{cases} f_{\mathrm{y,d}} \times A_{\mathrm{ef}} \\ \pi \times d \times l_a \times f_{\mathrm{vr,d}} \end{cases} \quad (13)$$

$$\begin{aligned} f_{\mathrm{y,d}} &= \frac{f_{\mathrm{y,k}}}{\gamma_{\mathrm{M,steel}}} \\ f_{\mathrm{vr,d}} &= \frac{f_{\mathrm{vr,la,dc,k}} \times k_{\mathrm{mod}}}{\gamma_{\mathrm{M,wood/adhesive}}} \end{aligned} \quad (14)$$

where $f_{\mathrm{y,d}}$ is the design of yield strength (N/mm^2) of steel rod; A_{ef} is the stress design relevant cross-section (mm^2) of steel rod; $f_{\mathrm{vr,d}}$ is the design value of bond shear strength (N/mm^2); $f_{\mathrm{y,k}}$ is the characteristic value of yield strength (N/mm^2) of steel rod; $\gamma_{\mathrm{M,steel}}$ is the partial safety factor for steel rod, taken from (EN 1993-1-1, 2022); $\gamma_{\mathrm{M,wood/adhesive}}$ is the partial safety factor for wood, taken from (EN 1995-1-1, 2004); k_{mod} is the modification factor for load duration and service class, taken from (EN 1995-1-1, 2004); and $f_{\mathrm{vr,la,dc,k}}$ is the declared characteristic bond shear strength declared by the adhesive manufacturer. The following parameters were assumed in this paper: $\gamma_{\mathrm{M,steel}} = 1.0$, $\gamma_{\mathrm{M,wood/adhesive}} = 1.25$, $k_{\mathrm{mod}} = 0.6$, $f_{\mathrm{vr,la,dc,k}} = 21.3$ MPa.

BS EN 17334 also provides a formula for predicting the load carrying capacity of glued rods perpendicular to the grain, as shown in Eq. 15:

$$F_{90,\mathrm{Rd}} = \frac{F_{90,\mathrm{Rk}} \cdot k_{\mathrm{mod}}}{\gamma_{\mathrm{M}}}$$
$$F_{90,\mathrm{Rk}} = 14 \cdot b \sqrt{\frac{l_a}{\left(1 - \frac{l_a}{h}\right)}} \quad (15)$$

where b is the width and h is the length of specimen. The parameters were assumed in this paper: b = 105 mm, h = 400 mm.

Yeboah *et al*. (2013) Proposal

Yeboah *et al*. (2013) investigated the structural capacity of glued-in basalt fiber-reinforced polymer (BFRP) rods perpendicular to the grain in glulam. The main parameter investigated was the thickness of the glue layer from 2 mm to 12 mm and presented an equation for the pull-out load capacity perpendicular to the grain, as shown in Eq. 16:

$$F_{\mathrm{Y}} = f_{\mathrm{v,90,mean}} \cdot \pi \cdot d_{\mathrm{h}} \cdot l_{\mathrm{a}} \quad (16)$$

where $f_{\mathrm{v,90,mean}}$ = 5.7 MPa, l_{a} means embedment length, and d_{h} represents the diameter of the hole.

Comparison between Experimental Results and Prediction Models

Figures 11a and 11b depict the comparison between the predicted results for the GiR connections parallel to the grain and the average experimental results. Solid squares indicate the mean value of the test and hollow squares are the test values. For the S12-P series of specimens, while EN 17334-2021 (2021) proposal and GIROD predictive model provided a more reasonable prediction of pull-out strength when the embedment length is 60 mm, only DIN 1052 remained conservative as the embedment length increased. This conservatism is necessary due to the high dispersion of GiR connection strengths in CLT. The prediction for the S16-P series specimens was similar; most of the predictions were valid when the embedment length was low (< 10 d), but the prediction decreased progressively as the embedment length increases.

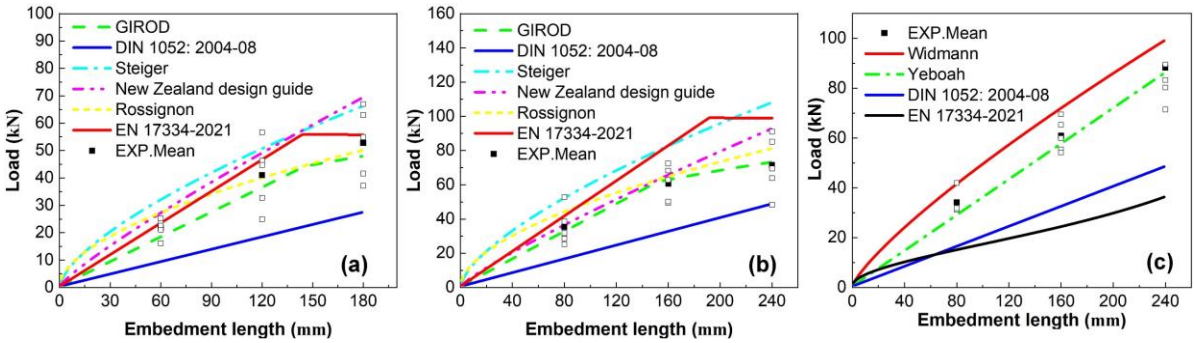

Fig. 11. Comparison between experimental results and the theoretical predictions: (a) S12-P series; (b) S16-P series; and (c) S16-PP series.

According to the results, DIN 1052 can relatively well predict the pull-out load of GiR connections in CLT compared to other theories. However, the use of the pull-out configuration may lead to discrepancies between the predicted and actual pull-out loads, especially since it is uncertain whether this approach prevents the emergence of certain failure modes of GiR connections in CLT that could lead to an overestimation of the pull-out loads, warranting further investigation in the future.

With most theories focusing on GiR connections parallel to the grain, and fewer design equations available for GiR connections perpendicular to the grain, a comparison of these limited theories with the experimental results is presented in Fig. 11. The theoretical model proposed by Yeboah *et al*. (2013) demonstrated better predictive capability for the pull-out load of GiR connections in CLT. Similarly, the proposed formula in DIN 1052 provided relatively conservative predictions. Because this investigation did not focus on the effect of failure modes on GiR connections in CLT, while it is known from the test results that failures due to different causes may have an impact on the final load carrying capacity, it is necessary to pay corresponding attention in future studies.

CONCLUSIONS

This study presented an experimental campaign on the glued-in rod (GiR) connections in cross-laminated timber (CLT), aiming to evaluate the pull-out performance of GiR in CLT. Forty-five specimens were tested with the main parameters including rod diameter, embedment length, and rod-to-grain angle. The main conclusions obtained are as follows.

1. Embedment length significantly impacted the behavior of GiR connections in CLT. Increasing the embedment length from 5 *d* to 15 *d* effectively enhanced the pull-out load, while the withdrawal stiffness remained relatively unchanged. The rod diameter also considerably influenced the bond strength of GiR connections. Specimens with a 16 mm rod diameter demonstrated a 62%, 47%, and 35% increase in pull-out load for embedment lengths of 5 *d*, 10 *d*, and 15 *d*, respectively, compared to those with a 12 mm rod diameter. It should be noted that the grade 8.8 steel rod used in this study did not yield; thus, adopting low-carbon soft steel rods for more detailed analysis is recommended for future research to better understand the ductility of connections.

2. The CMR model and the model proposed by Ling *et al.* (2014) were found to effectively predict the bond-slip behavior of GiR connections in CLT, offering valuable references for subsequent studies. However, further research is needed to expand the dataset and enhance the understanding of the bond behavior in CLT.
3. Most existing pull-out load prediction models tend to overestimate the pull-out load of GiR connections parallel to the grain in CLT. In contrast, the DIN 1052 model demonstrated greater accuracy and reliability in predicting the pull-out load of GiR connections in CLT, with some conservativeness that enhances its practical applicability.
4. The properties of timber, particularly its shear and rolling strengths, significantly influence the failure modes of GiR connections perpendicular to the grain in CLT. Future research should focus on more specific analyses of these influences, along with the development of refined prediction models that account for the unique mechanical behavior of CLT and the specific failure modes of GiR connections. Additionally, the study's limitations, including specimen size constraints and the push-pull test setup, highlight the need for further experimental work to capture the full range of failure modes and mechanical responses in CLT structures.

ACKNOWLEDGMENTS

The authors greatly appreciate the financial support from the National Natural Science Foundation of China (Grant No. 52108253), the Postgraduate Research Innovation Program of Jiangsu Province, China (Grant No. KYCX22_3285), the Natural Science Foundation of Jiangsu Province, China (Grant No. BK20221387) and the Key Laboratory of Building Structural Retrofitting and Underground Space Engineering (Shandong Jianzhu University), and Ministry of Education (Grant No. MEKL202306).

REFERENCES CITED

ASTM D1761-20 (2006). "Standard test methods for mechanical fasteners in wood and wood-based materials," ASTM International West Conshohocken, United States.

Ayansola, G. S., Tannert, T., and Vallee, T. (2022). "Experimental investigations of glued-in rod connections in CLT," *Construction and Building Materials* 324, article 126680. DOI:10.1016/j.conbuildmat.2022.126680

Azinović, B., Danielsson, H., Serrano, E., and Kramar, M. (2019). "Glued-in rods in cross laminated timber – Numerical simulations and parametric studies," *Construction and Building Materials* 212, 431-441. DOI: 10.1016/j.conbuildmat.2019.03.331

Azinović, B., Serrano, E., Kramar, M., and Pazlar, T. (2018). "Experimental investigation of the axial strength of glued-in rods in cross laminated timber," *Materials and Structures* 51(6). DOI: 10.1617/s11527-018-1268-y

Bengtsson, C., and Johansson, C.-J. (2002). "GIROD-Glued in rods for timber structures," SMT4-CT97-2199, Bengtsson, Charlotte.

Borgström, E., and Fröbel, J. (2019). *CLT Handbook: CLT Structures – Facts and Planning*, Stockholm: Skogsindustrierna Svenskt Trä.

Buchanan, A. (2007). *Timber Design Guide*, New Zealand Timber Industry Federation Inc, Wellington, New Zealand.

Cosenza, E., Manfredi, G., and Realfonzo, R. (1997). "Behavior and modeling of bond of FRP rebars to concrete," *Journal of Composites for Construction* 1(2), 40-51.

Coureau, J. L., Galimard, P., Cointe, A., Lartigau, J., and Morel, S. (2016). "Resistance-curves and wood variability: Application of glued-in-rod," *International Journal of Adhesion and Adhesives* 70, 1-9. DOI:10.1016/j.ijadhadh.2016.04.015

DIN 1052: 2004-08 (2008). "Berechnung und bemessung von holzbauwerken (Calculation and design of timber structures)," in: *Allgemeine Bemessungsregeln und Bemessungsregeln für den Hochbau* (*General Design Rules and Design Rules for Building Construction*), Berlin, Deutschland.

Eligehausen, R., Popov, E. P., and Bertero, V. V. (1983). "Local bond stress-slip relationships of deformed bars under generalized excitations: Experimental results and analytical model," in: *NTIS, 1983* (Report / Earthquake Engineering Research Center, Berkeley, California: 83, 23). DOI: 10.18419/opus-8473.

EN 1995-1-1 (2004)."Eurocode 5 : Design of timber structures. Part 1-1 : General Common rules and rules for buildings," British Standards Institution, Brüssel, Belgien.

EN 17334: 2021 (2021). "Glued-in rods in glued structural timber roducts-Testing, requirements and bond shear strength classification," British Standards Institution, Brüssel, Belgien.

EN 1993-1-1 (2022). "Eurocode 3 : Design of steel structures. Part 1-1 : General rules and rules for buildings," British Standards Institution, Brüssel, Belgien.

Estévez Cimadevila, J., Otero Chans, D., and Martín Gutiérrez, E. (2013). "Adhesive multi-bulbs: A novel anchoring system using threaded steel rods glued into wood," *Construction and Building Materials* 48, 131-136. DOI: 10.1016/j.conbuildmat.2013.06.079

Gagnon, S., and Pîrvu, C. (2011). *CLT Handbook : Cross-Laminated Timber*, FPInnovations and Binational Softwood Lumber Council, Quebec, Canada.

Gardelle, V., and Morlier, P. (2006). "Geometric parameters which affect the short term resistance of an axially loaded glued-in rod," *Materials and Structures* 40(1), 127-138. DOI:10.1617/s11527-006-9155-3

GB/T 7124-2008 (2008). "Adhesives - Determination of tensile lap-shear strength of rigid-rigid bonded assemblies," China Architecture and Building Press, China.

GB/T 3098.1-2010 (2010). "Mechanical properties of fasteners-Bolts, screws and studs," China Architecture and Building Press, China.

GB/T 1927.4-2021 (2021). "Test method for physical and mechanical properties of small clear wood specimens - Part 4: Determination of moisture content," China Architecture and Building Press, China.

Grunwald, C., Vallée, T., Fecht, S., Bletz-Mühldorfer, O., Diehl, F., Bathon, L., and Myslicki, S. (2019). "Rods glued in engineered hardwood products part II: Numerical modelling and capacity prediction," *International Journal of Adhesion and Adhesives* 90, 182-198. DOI:10.1016/j.ijadhadh.2018.05.004

Gustafsson, P. J., and Serrano, E. (2002). *Glued-in Rods for Timber Structures - Development of a Calculation Model (TVSM-3000; No. TVSM-3056)*. Division of Structural Mechanics, LTH.

Hassanieh, A., Valipour, H. R., Bradford, M. A., and Jockwer, R. (2018). "Glued-in-rod timber joints: analytical model and finite element simulation," *Materials and*

Structures 51(3). DOI:10.1617/s11527-018-1189-9

Hegeir, O. A., and Stamatopoulos, H. (2023). "Experimental investigation on axially-loaded threaded rods inserted perpendicular to grain into cross laminated timber," *Construction and Building Materials* 408, article 133740. DOI: 10.1016/j.conbuildmat.2023.133740

Koets, R. (2012). *Hoogbouw met Cross Laminated Timber*. Eindhoven: Technische Universiteit Eindhoven.

Lartigau, J., Coureau, J.-L., Morel, S., Galimard, P., and Maurin, E. (2014). "Mixed mode fracture of glued-in rods in timber structures," *International Journal of Fracture* 192(1), 71-86. DOI:10.1007/s10704-014-9986-9

Ling, Z., Xiang, Z., Liu, W., Yang, H., and Tang, J. (2019). "Load-slip behaviour of glue laminated timber connections with glued-in steel rod parallel to grain," *Construction and Building Materials* 227, article 117028. DOI:10.1016/j.conbuildmat.2019.117028

Ling, Z., Yang, H., Liu, W., Lu, W., Zhou, D., and Wang, L. (2014). "Pull-out strength and bond behaviour of axially loaded rebar glued-in glulam," *Construction and Building Materials* 65, 440-449. DOI:10.1016/j.conbuildmat.2014.05.008

Ling, Z., Yang, H., Liu, W., Zhu, S., and Chen, X. (2018). "Local bond stress-slip relationships between glue laminated timber and epoxy bonded-in GFRP rod," *Construction and Building Materials* 170, 1-12. DOI: 10.1016/j.conbuildmat.2018.03.052

Madhoushi, M., and Ansell, M. P. (2017). "Effect of glue-line thickness on pull-out behavior of glued-in GFRP rods in LVL: Finite element analysis," *Polymer Testing* 62, 196-202. DOI:10.1016/j.polymertesting.2017.06.029

Muciaccia, G. (2017). "An experimental approach to determine pull-out strength of single and multiple axially loaded steel rods bonded in glulam parallel to the grain," *Wood Material Science and Engineering* 14(2), 88-98. DOI: 10.1080/17480272.2017.1404491

Myslicki, S., Bletz-Mühldorfer, O., Diehl, F., Lavarec, C., Vallée, T., Scholz, R., and Walther, F. (2019). "Fatigue of glued-in rods in engineered hardwood products — Part I: Experimental results," *The Journal of Adhesion* 95(5-7), 675-701. DOI: 10.1080/00218464.2018.1555477

Myslicki, S., Vallée, T., Bletz-Mühldorfer, O., Diehl, F., Lavarec, L. C., and Créac'Hcadec, R. (2018). "Fracture mechanics based joint capacity prediction of glued-in rods with beech laminated veneer lumber," *The Journal of Adhesion* 95(5-7), 405-424. DOI: 10.1080/00218464.2018.1538879

Navaratnam, S., Thamboo, J., Ponnampalam, T., Venkatesan, S., and Chong, K. B. (2022). "Mechanical performance of glued-in rod glulam beam to column moment connection: An experimental study," *Journal of Building Engineering* 50, article 104131. DOI:10.1016/j.jobe.2022.104131

Otero Chans, D., Estévez Cimadevila, J., and Martín Gutiérrez, E. (2009). "Influence of the geometric and material characteristics on the strength of glued joints made in chestnut timber," *Materials and Design* 30(4), 1325-1332. DOI: 10.1016/j.matdes.2008.06.041

Otero Chans, D., Estévez Cimadevila, J., and Martín Gutiérrez, E. (2013). "Withdrawal strength of threaded steel rods glued with epoxy in wood," *International Journal of Adhesion and Adhesives* 44, 115-121. DOI:10.1016/j.ijadhadh.2013.02.008

Otero Chans, D., Estévez Cimadevila, J., and Martín Gutiérrez, E. (2011). "Strength of joints with epoxy-glued threaded steel rods in tali timber," *Journal of Materials in*

Civil Engineering 23(4), 453-458. DOI:10.1061/(asce)mt.1943-5533.0000191

Rajčić, V., Bjelanović, A., and Rak, M. (2006). *Comparison of the Pull-Out Strength of Steel Bars Glued in Glulam Elements Obtained Experimentally and Numerically*, Meeting of the CIB-W18,Florence, Italy.

Rossignon, A., and Espion, B. (2008). "Experimental assessment of the pull-out strength of single rods bonded in glulam parallel to the grain," *Holz als Roh und Werkstoff* 66(6), 419-432. DOI:10.1007/s00107-008-0263-3

Shekarchi, M., Farahani, E. M., and Oskouei, A. V. (2019). "Effect of seawater on pull-out behavior of glued-in single rods set parallel to the grain of timber joints," *Construction and Building Materials* 222, 342-357. DOI: 10.1016/j.conbuildmat.2019.06.140

Siha, A., and Zhou, C. (2021). "Pull-out tests on bond behavior between timber and near-surface-mounted steel bars," *Construction and Building Materials* 288, article 122974. DOI:10.1016/j.conbuildmat.2021.122974

Sofi, M., Lumantarna, E., Hoult, R., Mooney, M., Mason, N., and Lu, J. (2021). "Bond strength of GiR in cross-laminated timber: A preliminary study," *Construction and Building Materials* 301, article 123864. DOI:10.1016/j.conbuildmat.2021.123864

Steiger, R., Gehri, E., and Widmann, R. (2006). "Pull-out strength of axially loaded steel rods bonded in glulam parallel to the grain," *Materials and Structures* 40(1), 69-78. DOI:10.1617/s11527-006-9111-2

Steiger, R., Serrano, E., Stepinac, M., Rajčić, V., O'Neill, C., McPolin, D., and Widmann, R. (2015). "Strengthening of timber structures with glued-in rods," *Construction and Building Materials* 97, 90-105. DOI:10.1016/j.conbuildmat.2015.03.097

Stepinac, M., Rajčić, V., Hunger, F., and van de Kuilen, J. W. G. (2016). "Glued-in rods in beech laminated veneer lumber," *European Journal of Wood and Wood Products* 74(3), 463-466. DOI:10.1007/s00107-016-1037-y

Tannert, T., Zhu, H., Myslicki, S., Walther, F., and Vallée, T. (2016). "Tensile and fatigue investigations of timber joints with glued-in FRP rods," *The Journal of Adhesion* 93(11), 926-942. DOI:10.1080/00218464.2016.1190653

Tlustochowicz, G., Serrano, E., and Steiger, R. (2010). "State-of-the-art review on timber connections with glued-in steel rods," *Materials and Structures* 44(5), 997-1020. DOI: 10.1617/s11527-010-9682-9

Vallée, T., Rakesh, H. R., and Tannert, T. (2022). "Load-carrying capacity prediction of single rods glued into cross-laminated timber," *European Journal of Wood and Wood Products* 80(5), 1041-1055. DOI:10.1007/s00107-022-01835-1

Widmann, R., Steiger, R., and Gehri, E. (2007). "Pull-out strength of axially loaded steel rods bonded in glulam perpendicular to the grain," *Materials and Structures* 40(8), 827-838. DOI:10.1617/s11527-006-9214-9

Yeboah, D., Taylor, S., McPolin, D., and Gilfillan, R. (2013). "Pull-out behaviour of axially loaded Basalt Fibre Reinforced Polymer (BFRP) rods bonded perpendicular to the grain of glulam elements," *Construction and Building Materials* 38, 962-969. DOI: 10.1016/j.conbuildmat.2012.09.014

Zhang, H., Li, H., Dauletbek, A., Lorenzo, R., Corbi, I., and Corbi, O. (2023). "Research status of glued-in rods connections in wood structures," *Journal of Building Engineering* 65, article 105782. DOI:10.1016/j.jobe.2022.105782

Zhu, H., Faghani, P., and Tannert, T. (2017). "Experimental investigations on timber joints with single glued-in FRP rods," *Construction and Building Materials* 140, 167-172. DOI: 10.1016/j.conbuildmat.2017.02.091

Article submitted: April 22, 2025; Peer review completed: May 10, 2025; Revised version received and accepted: May 11, 2025; Published: May 14, 2025.
DOI: 10.15376/biores.20.3.5407-5428